Low field MRI RF coils and SNR improvement

Parsa, J.

Chapter 1

General Introduction

1.1 Magnetic Resonance Imaging (MRI) Systems

MRI is one of the most important medical imaging modalities in modern diagnostic medicine, known for its ability to produce detailed 3D images of internal soft tissue without using any harmful radiation, in contrast to X-ray, CT, and PET. Since the creation of the first Nuclear Magnetic Resonance (NMR) image in 1973 [1] MRI has been improved by academic and industrial groups in both hardware and software to enhance image quality and shorten scan times [2]. Clinical MRI systems operate at magnetic field strengths typically ranging from 0.5 to 3 Tesla (T), while human research systems are approaching 14 T. Higher static magnetic field (B_0) improves the image signal-to-noise ratio (SNR) [3].

However, moving towards a higher magnetic field also has downsides. Higher field MRI systems can cost more than a million euros per Tesla. In addition, a fixed and expensive site is needed to locate the system, together with costly maintenance, which makes these systems inaccessible. According to the World Health Organization, the majority of people worldwide have little or no access to an MRI. Even in developed countries, waiting times for an MRI scan can be up to several weeks [4,5]. In some countries, where MRI scan costs are partially or not covered by insurance companies [6] MRI is even less achievable.

Despite being intrinsically non-invasive, some safety factors are critical, such as radio frequency (RF) absorption power, strong magnetic field, and fast changes in gradient coil electrical current. Specific absorption rate (SAR) is an indication factor of maximum induced RF power in the human body, and peripheral nerve stimulation (PNS) is a limitation factor for rapid changes in gradient electrical currents. The safe operation limit for both factors is predefined in the scanner based on previous research and subject specifications. On the other hand, before each scan, the subject must be MR-safe, which means no magnetic-sensitive objects or implants are allowed in the scanner room. However, these days, most of the implants are MR safe, still some artifacts can present in the image around it, and besides that extra SAR safety needs to be considered.

The progress in cost efficiency, accessibility, and patient comfort has attracted researchers' attention to low-field (<0.1T) and mid-field MRI (~0.6 T) in recent years [7–9]. Modern hardware designed for specific body anatomies enables the creation of compact, portable, and POC MRI systems. These systems allow imaging in locations that traditional MRI machines

cannot reach, such as intensive care units (ICUs) [10,11], ambulances [12], and rural low-resource environments [13,14].

1.2 Low-Field MRI Systems

Figure 1.1 represents four different types of mid-field and low-field MRI systems. Figure 1.1a shows a full-body mid-field 0.55 T Siemens scanner: this system can be used primarily to reduce purchase, maintenance, and infrastructural costs, and increase availability for patients with contraindications such as medical implants, compared to conventional (1.5–3 T) field strengths. Mid-field MRI systems rely on superconductive materials within a cryogenic setup to generate the main magnetic field (B_0). In contrast, most low-field MRI systems utilize permanent magnets.

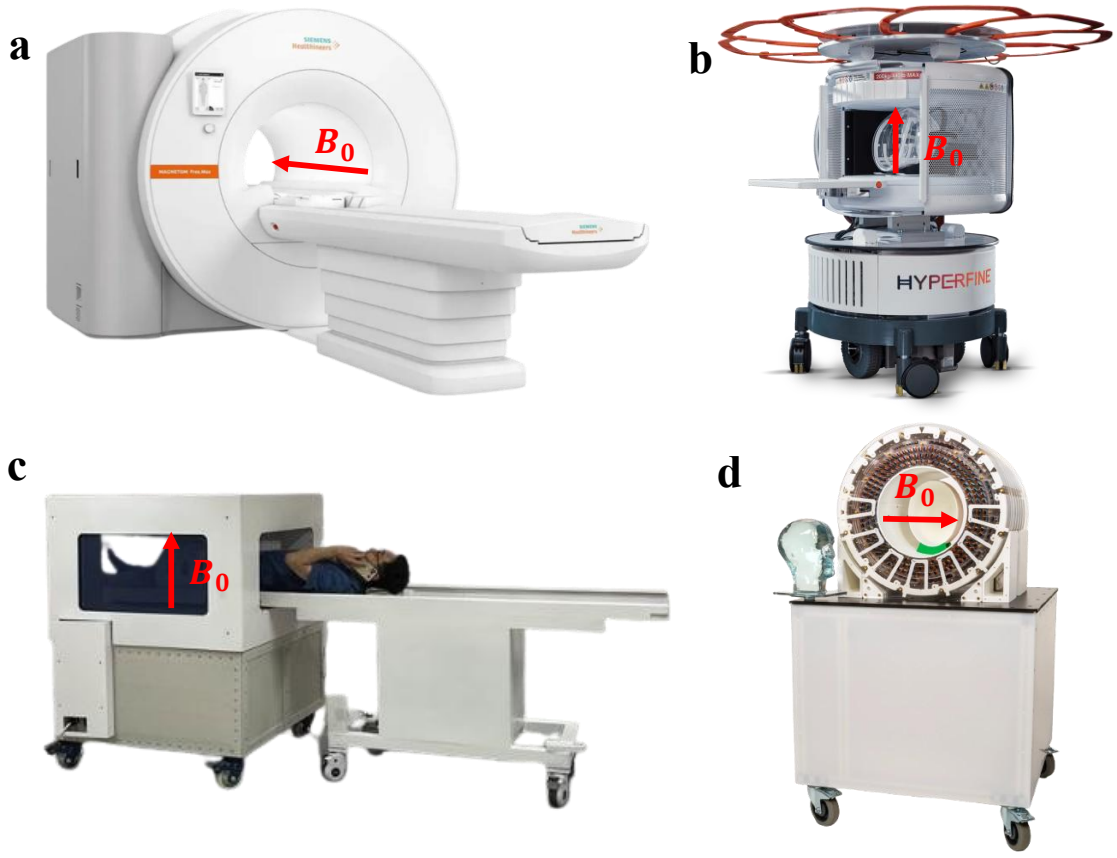

Figure 1.1. Two commercial (a, b) and two academic (c, d) MRI systems, one mid-field (a) and three low-field (b, c, d) systems. B_0 direction for each magnet configuration indicated in red. a) Siemens 0.55 T MAGNETOM Free.max full body system, which uses a resistive magnet and has the B_0 field direction along the axis of the bore. b) Hyperfine swoop, which has a field strength of 0.065 T and uses a parallel plate design, resulting in a B_0 field in the vertical direction. c) University of Hong Kong 0.055T system same magnet type as Hyperfine swoop. d) LUMC 0.046 T Halbach-array based system, which has a cylindrical bore and the B_0 field in the left-right direction.

This work focuses on POC MRI systems, where permanent magnets offer a cost-effective and power-free alternative to superconductive magnets, making them ideal for portable applications. These systems are normally in two categories: yoke design and Halbach-array base design. Figure 1.1b-d shows POC low-field systems from 50 mT to 64 mT, which are designed to be portable and increase accessibility of MRI by enabling it to be used in situations in which it has not previously been possible: examples include intensive care units. Unlike conventional systems, the main magnetic field of these systems is not aligned with the patient's body and is perpendicular to it (see Figure 1.1).

POC yoke-based MRI systems have an open entrance. These systems use two plates with disk-shaped permanent magnets separated by a ferromagnetic yoke, such as steel. Figure 1.1 shows such a system. Systems using this design have been mainly developed for neuroimaging [10,15] and, in recent work, for whole-body imaging [16]. These systems benefit from high B_0 homogeneity and a wide entrance, which enables the system to scan other parts of the body than only the brain. However, using a magnetic yoke reduces the mobility of these systems, and an extra electrical carrier system is needed to move these systems around. In addition, in yoke-based systems, plate-based gradients are used and these gradients are not efficient compared to normal cylindrical geometry gradients.

Another approach to designing a permanent magnet-based MRI system is to position a large number of small permanent magnets in specific orientations to create a Halbach array. This concept was originally proposed by Halbach [17] and developed by Blumler's group in particular (see Figure 1.1) [18–20]. These systems typically consist of multiple rings with varying diameters, made up of small magnets aligned in a Halbach-array orientation, resulting in a transverse B_0 field direction. Most implementations of this design are developed by research groups, with commercial versions still in progress. Unlike yoke-based systems, these systems have a cylindrical shape and are lightweight due to the absence of a ferromagnetic yoke. Moreover, these systems use cylindrical gradient coils, which are more efficient [21–23] and provide a more effective electromagnetic interference shielding environment due to their inner cylindrical shield. However, Halbach-array systems have some disadvantages, such as less B_0 uniformity due to complexity and manufacturing imperfections, compared with the yoke base systems. More detailed information on these systems will be presented in the subsequent chapters.

1.3 Radio Frequency (RF) Coils in MRI Systems

RF coils are an essential component of MRI systems for propagating RF signals in subjects. RF coils can have different shapes and sizes based on application, and they can be used in only transmit, only receive, or both transmit and receive modes. The quality of an MR image heavily depends on the design and placement of the RF coil, as it directly affects the SNR of images.

An RF transmit coil (Tx) generates an RF pulse that produces a small magnetic field (B_1^+) perpendicular to the B_0. This action of the RF pulse applied along one axis produces a torque perpendicular to that axis. As shown in Figure 1.2(b), the angle α by which the magnetization is rotated is proportional to the product of the strength of the applied RF field and the time, τ_{B_1} , for which it is applied.

$$\alpha = \gamma B_1^+ \tau_{B_1} , \tag{1}$$

The Tx-Coils generate the electromagnetic B_1^+ field, which is perpendicular to the main (static) magnetic field B_0, and oscillates at the resonance frequency, also known as the Larmor Frequency ω_r. The Larmor frequency ω_r depends on the type of nucleus and the strength of the main magnetic field. The RF receive coil (Rx) detects the precessing magnetization, resulting in an induced voltage via electromagnetic induction and Faraday's law:

$$V = -\frac{\partial \Phi(t)}{\partial t} = -\frac{\partial}{\partial t}\int_{sample} \frac{B_1^-}{I} . M_{xy} dr , \tag{2}$$

where the coil sensitivity is defined as B_1^-/I, *i.e.* the B_1^- field produced per unit applied current and M_{xy} is the transverse magnetization. The induced V is the MR signal.

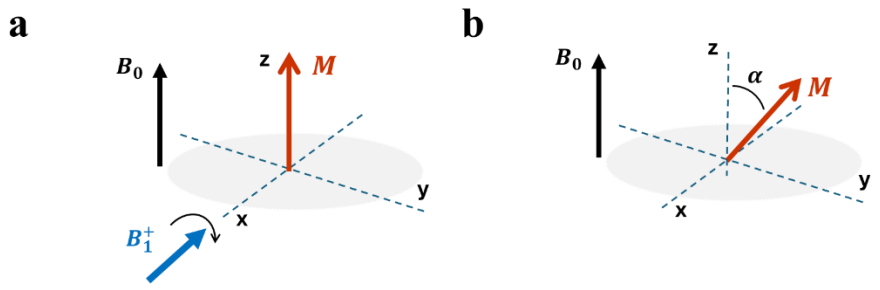

Figure 1.2. a) The effect of an RF pulse on the M is to rotate the magnetization about the axis along which B_1^+ is applied. b) The rotation angle α caused by RF pulse.

1.4 Radio Frequency Coil Specification

The geometry of the RF coil depends on the direction of the main magnetic field. In general, any coil geometry that creates a B_1 field perpendicular to the B_0 The field can be used in MRI systems, but several key factors must be taken into account. An ideal MRI RF coil should try to have these factors:

1- Create the highest transmit (B_1^+) magnetic field within the sample per unit input current to the coil.
2- Producing the minimum electric (E) field within the sample per unit input current to the coil.
3- For volume coils, creating B_1^+ field that is as homogeneous as possible across a large portion of the sample.

RF coils can have different designs and geometries based on their applications; some of the most common RF coils are shown in Figure 1.3.

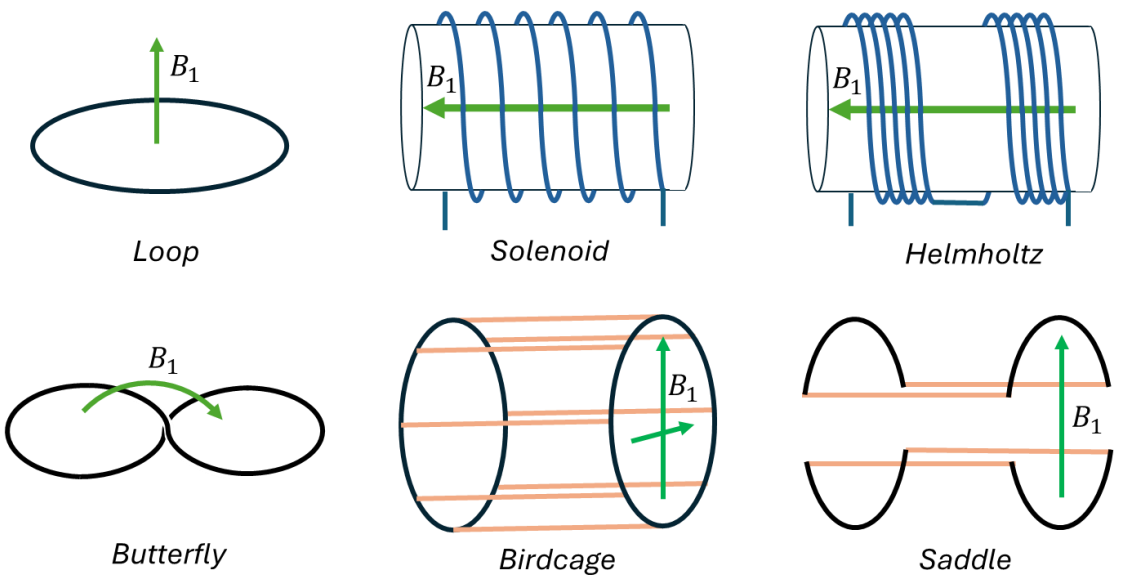

Figure 1.3. An illustration of different coil geometries is shown here. The B_1direction for each coil is indicated in green. Surface coils on the left and volume coils at the center and on the right.

1.5 SNR in MRI: A hardware perspective

Main magnetic field: Higher field strength inherently enhances the SNR due to increased magnetization, which amplifies the response signal. As Hoult established a theoretical study in early research [3], SNR scales approximately with $B_0^{\frac{3}{2}}$ at high magnetic field, which indicates that the higher the main magnetic field, the higher the SNR

RF coils: The design and quality of RF coils significantly affect the SNR. For both volume and surface coils, SNR has a direct relationship with the filling factor and the quality factor of the RF coil [24,25]. The filling factor represents spatial overlap between the RF coil's sensitive volume and the region of interest in the subject. A higher filling factor implies better coupling between the subject and the RF coil, which increases the amplitude of signal reception. In other words, by choosing a coil that fits closer to the region of interest (ROI), you potentially gain better images. The quality factor (Q) is a measure to compare coils in their efficiency to detect the MR signal. It is the ratio of the stored and dissipated energy in the coil. The Q-factor of a coil can be measured with and without the presence of a sample, which is called loaded and unloaded, respectively. The relation between the loaded Q and the unloaded Q is an indicator of the coil sensitivity.

$$Q_{ratio} = \frac{Q_{unloaded}}{Q_{loaded}}, \tag{3}$$

When the $Q_{ratio} < 1$ coil-noise dominates the sample noise, which results in reduced SNR. If $Q_{ratio} \gg 1$, the sample noise is dominant, and a reduction in coil losses would still improve the SNR, but quite small [26].

Receiver chain: Another major hardware component that affects the overall SNR in the system is the receiver chain. This consists of a transmit/receive switch when a single coil is used for transmit and receive, preamplifiers, and the analog-to-digital converter. Each component in the receive chain adds noise, which leads to a reduction in SNR [27]. The noise figure (F) of the receiver chain is a critical parameter, low noise figures result in enhancing SNR. Figure 1.4 shows a schematic of the Rx chain.

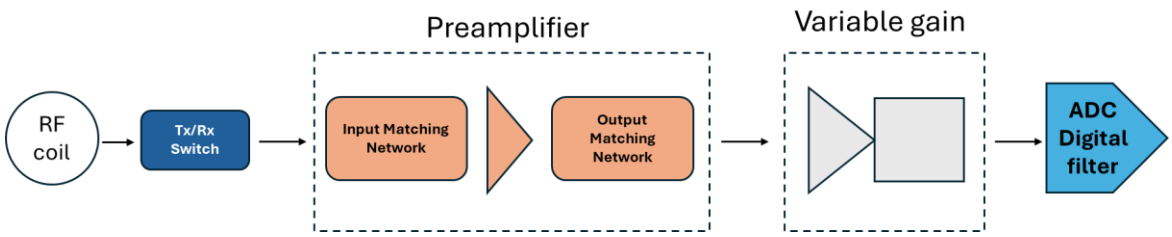

Figure 1.4. A schematic of the receiver chain. For a receive-only coil, the Tx/Rx switch can be removed if isolation is sufficient.

Gradient Systems: Gradient coils are essential for spatial encoding in MRI. However they do not directly contribute to SNR, their performance affects SNR indirectly through factors such as eddy currents and gradient-induced noise [28]. Gradients directly determine the resolution in an MRI image by their influence on k-space. The spatial frequency coordinate $k_x(t)$ is defined by the time integral of the gradient waveform:

$$k_x(t) = \frac{\gamma}{2\pi} \int_0^t G_x(t')\, dt' , \tag{4}$$

where γ is the gyromagnetic ratio and $G_x(t')$ is the applied gradient. The resolution Δx is inversely proportional to the maximum spatial frequency encoded:

$$\Delta x \approx \frac{1}{2k_{x,max}} , \tag{5}$$

which is set by the gradient strength and duration, and can be defined as: $k_{x,max} = \frac{\gamma}{2\pi} G_x T_{read}$.

Hence, stronger gradients enable broader k-space coverage in less time, thereby improving spatial resolution. In conventional MRI systems, high-resolution imaging in the sub-millimeter range is achievable due to high $k_{x,max}$ coverage within a short echo time. However, point-of-care (POC) MRI systems typically have much weaker gradient strengths (e.g., < 20 mT/m), reducing $k_{x,max}$, which increases voxel size and limits resolution. To compensate, one must increase readout times, which leads to longer echo times and signal decay, further compromising image quality. As a result, the lower gradient strength in POC devices imposes a fundamental limitation on achievable spatial resolution due to constrained k-space encoding capabilities [29].

1.6 Specific Absorption Rate (SAR)

The SAR describes the potential heating of a patient's tissue due to the interaction of the transmit coil's electric fields with electrically conductive tissue in the body and can be defined as:

$$SAR = \frac{\sigma|E|^2}{\rho}\ , \tag{6}$$

where σ is the electric conductivity of tissue (S/m), $|E|$ electric field magnitude, and ρ mass density of tissue [30]. The fact that RF transmit coils can deposit RF energy in the body as heat is often underestimated. At high field strengths (>1.5T), the RF signal wavelength is shorter than the body, leading to a safety concern of increased local RF power deposition within the body. The SAR distribution is governed by the subject's anatomy and tissue electrical properties, the RF coil design, and the characteristics of the applied RF pulse sequence. Moreover, SAR has a direct relationship with duty cycling and transmitted power, which can be defined as below for a rectangular RF pulse:

$$SAR = \frac{P_{ave}}{m} = \frac{P_{pulse} \times D}{m}\ , \tag{6}$$

where m is the mass of the subject, P_{pulse} is the peak transmitted power, and D is the duty cycling. To reduce SAR, the duty cycle and the power of the transmitted RF pulses can be reduced, at the cost of longer scan times and altered contrast. Regulatory standards define maximum permissible SAR levels for RF energy deposition in the body.

1.7 Low-Field MRI Systems and Challenges

POC MRI systems differ substantially from conventional MRI, from core hardware components to pulse-sequence design and post-processing. These differences introduce distinct technical and methodological challenges. To address these challenges and make these systems widely accessible, a new approach for each aspect is needed. In this thesis, I focus on challenges associated with RF coils and SNR in POC systems.

RF coils

Unlike conventional MRI, in most POC systems, the B_0 field has a transverse orientation, and the RF coils configuration is different between them. Figures 1.1 and 1.2 indicate B_0 and

B_1 directions in each system and coil geometry, respectively. The difference between B_0 direction allows POC systems to use a solenoidal base geometry for the RF coil. Because these systems are designed for partial-body application, different variations of the solenoid-based RF coil, which more closely fit the body part geometry, such as the head, are also commonly used. As Hoult [3] showed before, a solenoid is approximately two to three times more sensitive ($\frac{B_1}{I}$) than a linear saddle or birdcage coil, with a slightly poorer B_1 homogeneity measured over the active region of the coil. However, it is possible to use a saddle coil in these systems; the sensitivity, and consequently the SNR, would be much lower than that of a solenoidal-based coil.

SAR at low-field systems

Under conditions where tissue conductivity is frequency-independent and the RF skin depth is large compared to the object's dimensions, SAR scales with the square of the frequency, and it is typically considered negligible in POC systems. As a result, most publications do not account for SAR in POC systems. However, there are limiting factors related to the geometry of POC systems and the type of RF coils used, which may significantly influence this consideration. The compact design of Halbach POC systems is a key factor that enables their portability. This design results in the RF transmit coils fitting tightly around body parts like the head, causing strong local electric fields near the coil conductors to penetrate into the tissue around the skull.

Shielding and Electromagnetic Interference (EMI)

Unlike standard clinical scanners like 3T systems, one of the main challenges for all POC systems is designing them to operate outside the usual RF-shielded environment. In addition to the inherently low SNR in POC systems, the absence of an RF-shielded room makes these systems more vulnerable to EMI from nearby electronics, which further reduces the SNR. Addressing this challenge requires rethinking traditional EMI suppression techniques. A combination of active and passive shielding methods must be developed in innovative ways.

SNR optimization from the RF coil perspective

Halbach POC systems have some geometry limitations. Ideal Halbach POC systems should have infinite lengths to produce uniform B_0, however, in practice, this is not possible. For neuroimaging applications, the length of these systems should be considered as short as

possible because only the head and neck up to the subject's shoulder will be inside the scanner, and the rest of the body is outside of the scanner. As a result, finding a trade-off between the length and diameter of the Halbach POC system is critical. On the other hand, a conductor shield inside the magnet bore of Halbach POC systems is always used to prevent electromagnetic coupling between the gradient coil and the RF coil and to shield the RF coil from EMI. However, this shield reduces the efficiency of the RF coil. With this said, finding the optimum magnet diameter to get the optimum intrinsic SNR is important and needs to be investigated.

X nuclei imaging

There are other nuclei than ^{1}H with active isotopes in producing MR signal, however, they have a gyromagnetic ratio of less than ^{1}H. Isotope 19-fluorine (^{19}F) is the nucleus with the highest gyromagnetic ratio, approximately 91% that of ^{1}H. In biological applications, there is essentially zero background signal from ^{19}F, which provides high contrast when detecting ^{19}F molecules that have been introduced into the body. In the last 20 years, many investigations have been conducted for ^{19}F imaging at normal clinical MRI systems. On the other hand, because of the low main magnetic field at POC systems, the chemical shift in fluorinated pharmaceutical components is almost zero. This leads to studying the opportunities and challenges of ^{19}F in POC systems.

1.8 Outline of this thesis

This thesis aims to address the challenges associated with RF coils for POC Halbach-based systems. Chapter 2 investigates the SAR limits of common RF coils used in these systems for high-intensity RF sequences such as fast spin-echo. In Chapter 3, a new method is introduced to mitigate EMI in POC systems and to improve image SNR. This is followed by Chapter 4, which studies optimization of intrinsic SNR for Halbach-based POC systems from the perspectives of the main magnet and RF coil. Chapter 4 examines opportunities to use 19F nuclei as a contrast agent for POC systems. Finally, Chapter 5 presents a general discussion of the results across all chapters and explores the remaining challenges and future research directions.

References

1) Lauterbur PC. Image Formation by Induced Local Interactions: Examples Employing Nuclear Magnetic Resonance. Nature 1973;242:190–1. https://doi.org/10.1038/242190a0.
2) Börnert P, Norris DG. A half-century of innovation in technology-preparing MRI for the 21st century. Br J Radiol 2020;93:20200113. https://doi.org/10.1259/bjr.20200113.
3) Hoult DI, Richards RE. The signal-to-noise ratio of the nuclear magnetic resonance experiment. J Magn Reson 1969 1976;24:71–85. https://doi.org/10.1016/0022-2364(76)90233-X.
4) Anazodo UC, Ng JJ, Ehiogu B, Obungoloch J, Fatade A, Mutsaerts HJMM, et al. A framework for advancing sustainable magnetic resonance imaging access in Africa. NMR Biomed 2023;36:e4846. https://doi.org/10.1002/nbm.4846.
5) Human Health Campus - Database & Statistics n.d. https://humanhealth.iaea.org/HHW/DBStatistics/IMAGINEMaps3.html (accessed February 11, 2025).
6) Chernew M, Cooper Z, Hallock EL, Scott Morton F. Physician agency, consumerism, and the consumption of lower-limb MRI scans. J Health Econ 2021;76:102427. https://doi.org/10.1016/j.jhealeco.2021.102427.
7) Wald LL, McDaniel PC, Witzel T, Stockmann JP, Cooley CZ. Low-cost and portable MRI. J Magn Reson Imaging 2020;52:686–96. https://doi.org/10.1002/jmri.26942.
8) Sarracanie M, Salameh N. Low-Field MRI: How Low Can We Go? A Fresh View on an Old Debate. Front Phys 2020;8:172. https://doi.org/10.3389/fphy.2020.00172.
9) Marques JP, Simonis FFJ, Webb AG. Low-field MRI: An MR physics perspective. J Magn Reson Imaging JMRI 2019;49:1528–42. https://doi.org/10.1002/jmri.26637.
10) Sheth KN, Mazurek MH, Yuen MM, Cahn BA, Shah JT, Ward A, et al. Assessment of Brain Injury Using Portable, Low-Field Magnetic Resonance Imaging at the Bedside of Critically Ill Patients. JAMA Neurol 2021;78:41. https://doi.org/10.1001/jamaneurol.2020.3263.
11) Turpin J, Unadkat P, Thomas J, Kleiner N, Khazanehdari S, Wanchoo S, et al. Portable Magnetic Resonance Imaging for ICU Patients. Crit Care Explor 2020;2:e0306. https://doi.org/10.1097/CCE.0000000000000306.
12) Nakagomi M, Kajiwara M, Matsuzaki J, Tanabe K, Hoshiai S, Okamoto Y, et al. Development of a small car-mounted magnetic resonance imaging system for human elbows using a 0.2 T permanent magnet. J Magn Reson San Diego Calif 1997 2019;304:1–6. https://doi.org/10.1016/j.jmr.2019.04.017.
13) K C, C C, Ms G, L V, Nf O, Dg P, et al. Implementation of a Low-Field Portable MRI Scanner in a Resource-Constrained Environment: Our Experience in Malawi. AJNR Am J Neuroradiol 2022;43. https://doi.org/10.3174/ajnr.A7494.
14) Obungoloch J, Muhumuza I, Teeuwisse W, Harper J, Etoku I, Asiimwe R, et al. On-site construction of a point-of-care low-field MRI system in Africa. NMR Biomed 2023;36:e4917. https://doi.org/10.1002/nbm.4917.
15) He Y, He W, Tan L, Chen F, Meng F, Feng H, et al. Use of 2.1 MHz MRI scanner for brain imaging and its preliminary results in stroke. J Magn Reson San Diego Calif 1997 2020;319:106829. https://doi.org/10.1016/j.jmr.2020.106829.

16) Zhao Y, Ding Y, Lau V, Man C, Su S, Xiao L, et al. Whole-body magnetic resonance imaging at 0.05 Tesla. Science 2024;384:eadm7168. https://doi.org/10.1126/science.adm7168.
17) Halbach K. Strong Rare Earth Cobalt Quadrupoles. IEEE Trans Nucl Sci 1979;26:3882–4. https://doi.org/10.1109/TNS.1979.4330638.
18) O'Reilly T, Teeuwisse WM, Webb A. Three-dimensional MRI in a homogenous 27 cm diameter Bore Halbach Array Magnet. J Magn Reson 2019;307:106578. https://doi.org/10.1016/j.jmr.2019.106578.
19) Cooley CZ, Haskell MW, Cauley SF, Sappo C, Lapierre CD, Ha CG, et al. Design of sparse Halbach magnet arrays for portable MRI using a genetic algorithm. IEEE Trans Magn 2018;54:5100112. https://doi.org/10.1109/TMAG.2017.2751001.
20) Cooley CZ, McDaniel PC, Stockmann JP, Srinivas SA, Cauley SF, Śliwiak M, et al. A portable scanner for magnetic resonance imaging of the brain. Nat Biomed Eng 2021;5:229–39. https://doi.org/10.1038/s41551-020-00641-5.
21) de Vos B, Fuchs P, O'Reilly T, Webb A, Remis R. Gradient Coil Design and Realization for a Halbach-Based MRI System. IEEE Trans Magn 2020;56:1–8. https://doi.org/10.1109/TMAG.2019.2958561.
22) de Vos B, Parsa J, Abdulrazaq Z, Teeuwisse WM, Van Speybroeck CDE, de Gans DH, et al. Design, Characterisation and Performance of an Improved Portable and Sustainable Low-Field MRI System. Front Phys 2021;9. https://doi.org/10.3389/fphy.2021.701157.
23) Turner R, Bowley RM. Passive screening of switched magnetic field gradients. J Phys [E] 1986;19:876. https://doi.org/10.1088/0022-3735/19/10/023.
24) Edelstein WA, Glover GH, Hardy CJ, Redington RW. The intrinsic signal-to-noise ratio in NMR imaging. Magn Reson Med 1986;3:604–18. https://doi.org/10.1002/mrm.1910030413.
25) Ocali O, Atalar E. Ultimate intrinsic signal-to-noise ratio in MRI. Magn Reson Med 1998;39:462–73. https://doi.org/10.1002/mrm.1910390317.
26) Gilbert K m., Scholl T j., Chronik B a. RF coil loading measurements between 1 and 50 MHz to guide field-cycled MRI system design. Concepts Magn Reson Part B Magn Reson Eng 2008;33B:177–91. https://doi.org/10.1002/cmr.b.20118.
27) Webb A, O'Reilly T. Tackling SNR at low-field: a review of hardware approaches for point-of-care systems. Magn Reson Mater Phys Biol Med 2023;36:375–93. https://doi.org/10.1007/s10334-023-01100-3.
28) de Vos B, Remis R, Webb A. Segmented RF shield design to minimize eddy currents for low-field Halbach MRI systems. J Magn Reson 2024;362:107669. https://doi.org/10.1016/j.jmr.2024.107669.
29) Handbook of MRI Pulse Sequences. 2004.
30) Fiedler TM, Ladd ME, Bitz AK. SAR Simulations & Safety. NeuroImage 2018;168:33–58. https://doi.org/10.1016/j.neuroimage.2017.03.035.
31) Chou CK, Bassen H, Osepchuk J, Balzano Q, Petersen R, Meltz M, et al. Radio frequency electromagnetic exposure: Tutorial review on experimental dosimetry. Bioelectromagnetics 1996;17:195–208. https://doi.org/10.1002/(SICI)1521-186X(1996)17:3<195::AID-BEM5>3.0.CO;2-Z.